Structural stability and thermal properties of BeO from the quasiharmonic approximation

2010 J. Phys.: Condens. Matter 22 045404

(http://iopscience.iop.org/0953-8984/22/4/045404)

IOP Publishing Journal of Physics: Condensed Matter

J. Phys.: Condens. Matter **22** (2010) 045404 (9pp) doi:10.1088/0953-8984/22/4/045404

Structural stability and thermal properties of BeO from the quasiharmonic approximation

Urszula D Wdowik

Institute of Technology, Pedagogical University, PL-30-084 Cracow, Poland

E-mail: sfwdowik@cyf-kr.edu.pl

Received 22 October 2009, in final form 14 December 2009
Published 12 January 2010
Online at stacks.iop.org/JPhysCM/22/045404

Abstract

The phase diagram and thermal properties of BeO crystal are calculated within the quasiharmonic approximation and using density functional theory. The wurtzite, zinc blende and rocksalt phases of BeO are considered. Phonons are calculated versus external pressure. The pressure dependence of frequencies for the zone-center phonon modes is analyzed. The resulting free energy provides predictions for the temperature dependence of various quantities such as the equilibrium volume, thermal expansivity and isobaric heat capacity. The mean-squared vibrations of BeO atoms are investigated as well. The calculated (p, T) diagram predicts a structural phase transition from the wurtzite to rocksalt phase solely. The zinc blende structure is energetically not preferred in the investigated range of pressures and temperatures. Theoretical results are compared with the available experimental data and other *ab initio* calculations. Existing discrepancies between quasiharmonic theory and experiment are discussed and some explanation is given.

1. Introduction

Insulating oxides have physical properties that make them useful in a wide range of applications. Unique properties of beryllium oxide, BeO, such as high thermal conductivity [1], high electrical resistivity [2], high thermal stability (melting temperature $T_m = 2550\,^{\circ}C$), high hardness [3] and radiation resistance have made it applicable as the principal reactor-moderating material [4] and chip carrier substrate for high-power applications. On the other hand, BeO is an interesting ceramic from a theoretical point of view as it is the only alkaline-earth oxide crystallizing in the hexagonal wurtzite structure, while other oxides in this family have the rocksalt structure.

Beryllium oxide has been a subject of several experimental and theoretical investigations [1–7, 9–23]. Many theoretical studies of BeO were focused on the pressure-induced phase transitions [15–18, 21, 22, 39]. The wurtzite structure (w-BeO) was expected to transform either to the zinc blende (z-BeO) or rocksalt (r-BeO) phase upon compression. A wurtzite–zinc blende–rocksalt sequence was also reported. Moreover, it has been found that z-BeO is a metastable phase with enthalpy very close to that of the w-BeO phase. Depending on the approximation used in first-principles calculations a significant discrepancy exists in prediction of the transition pressure. The w-BeO phase was expected to undergo transition to the r-BeO phase at 22 or 40 GPa [6, 15]. The intermediate z-BeO phase was reported to be stable above 74, 63–76 or 91 GPa before transforming to the r-BeO phase at 137, 95 or 147 GPa [17–19]. On the other hand, more recent calculations performed by Cai *et al* [21] do not predict the wurtzite–zinc blende–rocksalt phase transition sequence below 200 GPa. They suggest that around 105 GPa the w-BeO structure can transform directly to the r-BeO structure. A similar value of the wurtzite-to-rocksalt transition pressure (107 GPa) was obtained from the full-potential linearized-augmented plane-wave method [22]. These calculations predict also for the r-BeO phase to transform into the z-BeO phase above 110 GPa. Only a few experiments have been performed to look at the phase transitions in BeO [6, 12]. The static x-ray diffraction experiments [12] show no phase transition up to 126 GPa but they point out a new phase which appears around 137 GPa.

Most of the theoretical studies devoted to the phase stability of BeO upon pressure was limited to zero temperature and the role of the lattice vibrations in stabilizing one phase over the other at the given temperature and pressure was ne-

glected. In nonmetals such as BeO, phonons are the primary excitations that can influence its thermodynamical and transport properties. Behavior of the lattice vibrations under pressure can provide additional information about the structural stability and phase transformation [24–26]. Vibrational properties of BeO have been studied experimentally by infrared [4] and Raman spectroscopy [4, 6, 27–30] as well as by inelastic neutron [31, 32] and x-ray scattering [33]. For the w-BeO structure some preliminary calculations of the phonon dispersion relations have been done using phenomenological models [32, 34] and recently within the *ab initio* approach [33, 35]. In the latter case, phonons were obtained only for the ground state.

The main aim of the present work is to extend the description of BeO properties to finite temperatures using the approach of the quasiharmonic approximation. Phonons are calculated as a function of external pressure for wurtzite, zinc blende and rocksalt phases. Some selected thermal properties of this compound, e.g. Gibbs free energy, volume thermal expansion, and heat capacities at constant volume and pressure, are investigated and compared to the available experimental data. Relying on the calculated quasiharmonic Gibbs free energies the (p, T) phase diagram is constructed and the structural stability of BeO is analyzed.

2. Methodology

Ab initio calculations of wurtzite, zinc blende and rocksalt phases of BeO were performed within density functional theory, using the pseudopotential method with the generalized gradient approximation (GGA) implemented in the VASP code [36, 37]. Vanderbilt-type ultrasoft pseudopotentials provided by VASP were used for beryllium and oxygen atoms. These pseudopotentials represent (s^2p^0) and (s^2p^4) electron configurations of Be and O atoms, respectively. A plane-wave expansion up to 515 eV was used. All calculations were done with $2 \times 2 \times 2$ supercells containing 48, 64 and 64 atoms for w-BeO, z-BeO and r-BeO phases, respectively. The Brillouin zone was sampled using the $2 \times 2 \times 2$ k-point mesh generated by the Monkhorst–Pack scheme. A combination of conjugate gradient energy minimization and a quasi-Newton force minimization was used to optimize geometry and the atomic positions of the supercells. The atomic positions were relaxed until the forces were smaller than 10^{-6} eV Å^{-1}. The total energy was converged down to 10^{-7} eV. External pressure was varied from -30 to 130 GPa.

Dynamical properties of the BeO phases were calculated using the direct method [38, 39] based on the forces calculated via the Hellmann–Feynman theorem. The non-vanishing Hellmann–Feynman (HF) forces acting on the atoms in the given supercell are generated when a single atom is displaced from its equilibrium position. For each phase of BeO, the HF forces were created by displacing crystallographically nonequivalent Be and O atoms from their equilibrium positions. The displacement amplitude of 0.03 Å was used. To minimize systematic error, both positive and negative displacements were applied. Therefore, 12, 4 and 4 displacements were calculated for w-BeO, z-BeO and r-BeO structures, respectively.

In the BeO crystal, the macroscopic electric field splits the infrared-active optical modes into transverse (TO) and longitudinal (LO) components. Frequencies of TO modes are calculated in a straightforward manner within the direct method but the LO modes can only be obtained via the introduction of the non-analytical term [40] into the dynamical matrix. In general, this term depends on the Born effective charge tensor $\mathbf{Z}^*$ and the electronic part of the dielectric function ϵ_∞ (high-frequency dielectric constant). For cubic phases of BeO (z-BeO and r-BeO) the symmetry reduces the tensor $\mathbf{Z}^*$ to a diagonal tensor with a single element $Z^*_{\mathrm{Be}} = -Z^*_{\mathrm{O}}$. In hexagonal symmetry such as in the w-BeO phase the tensor is diagonal and reduces to two components, i.e. parallel ($Z^*_\parallel$) and perpendicular ($Z^*_\perp$) to the c axis. Hence, the following relations apply: $Z^*_\parallel \equiv Z^*_{zz}(\mathrm{Be}) = -Z^*_{zz}(\mathrm{O})$ and $Z^*_\perp \equiv Z^*_{xx}(\mathrm{Be}) = Z^*_{yy}(\mathrm{Be}) = -Z^*_{xx}(\mathrm{O}) = -Z^*_{yy}(\mathrm{O})$. Effective charges were calculated for each phase at zero pressure using the Berry phase method. For w-BeO $Z^*_\perp = 1.85$ and $Z^*_\parallel = 1.97$ were obtained. They are comparable to those determined by Bosak *et al* [33] ($Z^*_\perp = 1.79$, $Z^*_\parallel = 1.85$) and stay in agreement with other *ab initio* calculations [35, 41–43]. The Born effective charges of 1.98 and 2.0 were obtained for z-BeO and r-BeO, respectively. The averaged value of the high-frequency dielectric constant of $\epsilon_\infty = 2.96$ has been taken from experiments performed by Loh [4]. In the present work, the Born effective charges and ϵ_∞ are assumed not to vary with the applied pressure. Such an approximation is supported by experiments and calculations carried out for AlN, GaN and ZnO compounds which predict for these materials a weak pressure dependence of $\mathbf{Z}^*$ and ϵ_∞ [44–46]. Therefore, the calculated LO–TO splitting is expected to show only a slight variation upon crystal compression. Moreover, the LO–TO splitting has negligible influence on the thermal properties of the material as the thermodynamical functions being derived from the phonon density of states are practically insensitive to the decrease or increase in the mode splitting with pressure [25, 47]. This is due to the fact that LO modes contribute very little to the phonon density of states as they differ from TO modes only in a small volume of the reciprocal lattice in the vicinity of the Γ-point.

To study the phase stability of the crystal and to construct the (p, T) diagram the quasiharmonic approximation was applied. In this approach a change of the crystal volume due to finite temperature is mapped to the change of the crystal volume at $T = 0$ K (typically as a function of pressure). Thermodynamical functions are calculated using standard formulae for harmonic crystals. Anharmonic effects are, to some extent, taken into account by the volume (pressure) dependence of the phonon frequencies. Phonon frequencies at constant volume are assumed to be independent of temperature. The relative change of the $(\mathbf{k}, j)$ mode frequency $\omega(\mathbf{k}, j)$ with volume V is usually described by the mode-specific Grüneisen parameter which is a dimensionless quantity defined as

$$\gamma(\mathbf{k}, j) = -\frac{\partial(\ln \omega(\mathbf{k}, j))}{\partial \ln V} = -\frac{V}{\omega(\mathbf{k}, j)}\frac{\partial \omega(\mathbf{k}, j)}{\partial V}. \qquad (1)$$

The thermal Grüneisen parameter $\gamma(T)$ can be obtained as the following average:

$$\gamma(T) = \frac{\sum_{\mathbf{k},j} \gamma(\mathbf{k}, j) C_V(\mathbf{k}, j)}{\sum_{\mathbf{k},j} C_V(\mathbf{k}, j)}, \tag{2}$$

where the contribution from each mode $(\mathbf{k}, j)$ is weighted by its contribution to the specific heat $C_V(\mathbf{k}, j)$. The denominator of the above equation equals the lattice contribution to the heat capacity at constant volume and it takes on the following form:

$$C_V = k_B \sum_{\mathbf{k},j} \left(\frac{\hbar\omega(\mathbf{k}, j)}{2k_B T} \right)^2 \frac{1}{\sinh^2(\hbar\omega(\mathbf{k}, j)/2k_B T)}, \tag{3}$$

where T is the temperature, and k_B and $\hbar$ denote the Boltzmann and Planck constants, respectively. One can also express C_V via the calculated phonon density of states $g(\omega)$. Hence, the equivalent form of equation (3) is given by

$$C_V = Nrk_B \int_0^\infty \mathrm{d}\omega\, g(\omega)(\hbar/k_B T) \frac{\exp(\hbar\omega/k_B T)}{[\exp(\hbar\omega/k_B T) - 1]^2}, \tag{4}$$

where N is the number of primitive unit cells and r stands for the number of degrees of freedom in the unit cell. In the (quasi)harmonic approximation the phonon density of states (implicitly depending on V) can be used to evaluate phonon-dependent thermodynamic quantities as a function of volume and temperature. In particular, the Helmholtz free energy of the material can be expressed in the following way:

$$F(V, T) = E(V) + F_{\mathrm{ph}}(V, T) = E(V) + k_B T \times \int_0^\infty g(\omega) \ln\left[2\sinh\left(\frac{\hbar\omega}{2k_B T} \right) \right], \tag{5}$$

where $E(V)$ is the energy of the motionless lattice obtained directly from *ab initio* calculations, while $F_{\mathrm{ph}}(V, T)$ denotes the vibrational free energy of a harmonic system. The term $F_{\mathrm{ph}}(V, T)$ includes the vibrational zero-point energy which remains finite for $T \to 0$. Any purely electronic contribution is neglected. One has to note that only $F_{\mathrm{ph}}(V, T)$ depends explicitly on temperature. At the given temperature T, the equilibrium volume follows from a minimization of $F(V, T)$ with respect to V.

The crystal equation of state can be obtained from the following expression:

$$p(V, T) = -\left[\frac{\partial F(V, T)}{\partial V} \right]_T, \tag{6}$$

with p denoting pressure. Under conditions of constant T and p, the thermodynamically stable phase is that with the lowest Gibbs free energy, defined as

$$G(T, p) = F(V, T) + pV. \tag{7}$$

Calculations of $G(T, p)$ have to be carried out for all phases under consideration. A coexistence of phases is indicated by the points on the (p, T) plane for which the difference between Gibbs free energies is equal to zero.

The calculated $F(V, T)$ can be used to study thermal properties and thermodynamic parameters of the crystal. The equation of state, given by relation (6), enables calculations of the thermal expansivity. The volume thermal expansion coefficient is defined as

$$\alpha_V(T) = \frac{1}{V} \left(\frac{\partial V}{\partial T} \right)_p. \tag{8}$$

In the quasiharmonic approximation the quantities α_V, C_V, γ and the isothermal bulk modulus $B_T = V(\partial^2 F(V, T)/\partial^2 V)_T$ are connected by the Grüneisen relation:

$$\gamma(T) = \frac{V\alpha_V B_T}{C_V}. \tag{9}$$

Thermal expansivity of a crystal leads to the difference between the heat capacity at constant pressure C_p and the heat capacity at constant volume C_V, which is given in the quasiharmonic approach by the following relationship:

$$C_p - C_V = \alpha_V^2(T) B V T. \tag{10}$$

The heat capacity C_V follows the Debye model and approaches the Dulong–Petit limit at high temperatures, while C_p increases linearly with T at high temperatures.

Technical details concerning the construction of the phase diagram using the quasiharmonic approximation can be found in [26].

3. Results and discussion

3.1. Structural properties of BeO phases and phase stability at $T = 0$ K

The calculated structural parameters of the w-BeO, z-BeO and r-BeO phases are listed in table 1. They result from the minimization of the supercell ground-state energies with respect to the electronic states and ionic configurations. The bulk modulus is derived from the least-squares fit of the $E(V)$ curve. It is assumed that the calculated data follow the Murnaghan equation of state. Table 1 also compares the calculated structural properties of BeO phases with the experimental data [3] and other first-principles calculations [19, 23]. One has to note that neither for z-BeO nor r-BeO do the experimental data exist. A comparison with other theoretical results is made only to the DFT calculations performed with the GGA approximation. Both theoretical results are very close to each other and they remain in good agreement with experiments. One observes a slight underestimation of the w-BeO bulk modulus as compared to the experimental data. The lattice constants of the w-BeO structure decrease monotonically with increasing pressure. For the w-BeO phase, the a axis is more compressible than the c axis, while the ratio c/a and the oxygen parameter do not vary with pressure. Results of the present calculations are very close to the experimental data reported by Hazen *et al* [3], which show practically isotropic compression of the w-BeO structure and the lack of pressure dependence of the oxygen parameter.

It is found that the w-BeO phase is lower in energy than the remaining phases. The difference between the ground-state energies of w-BeO and z-BeO is as small as

Table 1. Calculated and measured structural parameters, bulk moduli and axial compressibilities for wurtzite, zinc blende and rocksalt phases of BeO. Lattice constants, bulk modulus (B) and compressibilities (κ_a, κ_c) are given in (Å), (GPa) and (GPa^{-1}), respectively. Symbol x denotes the oxygen position in the w-BeO structure.

	Theory			Experiment (298 K)
	Present	Reference [19]	Reference [23]	Reference [3]
		w-BeO structure		
a (Å)	2.706	2.703	2.712	2.696
c/a	1.624	1.620	1.624	1.624
x	0.378	0.377	0.378	0.378
B	204	203	209	210
κ_a	1.51×10^{-3}	—	1.61×10^{-3}	1.50×10^{-3}
κ_c	1.45×10^{-3}	—	1.58×10^{-3}	1.46×10^{-3}
		z-BeO structure		
a	3.818	3.810	—	—
B	198	201	—	—
κ_a	1.49×10^{-3}			
		r-BeO structure		
a	3.647	3.648	—	—
B	229	231	—	—
κ_a	1.31×10^{-3}			

-13 meV/f.u., while the energy difference between w-BeO and r-BeO amounts to -1 eV/f.u.. The w-BeO and z-BeO structures are similar to each other as far as the second-nearest neighbors are concerned and hence such a small difference in their energies can be expected. Results of the present calculations are consistent with predictions of other *ab initio* results as well as experimental observations which indicate the wurtzite structure to be the most stable phase of the BeO crystal.

The phase transition pressure p_t is determined from the comparison of the Gibbs free energies of particular BeO phases. For the zero-temperature limit, the Gibbs free energy is simply the enthalpy of the system, i.e. $G(T = 0, p) = H(p) = E(V) + pV$. The enthalpies of the w-BeO, z-BeO and r-BeO phases increase gradually with increasing pressure. The enthalpy of w-BeO becomes equal to the enthalpy of z-BeO at 101 GPa. Above this pressure, the z-BeO structure is more stable than the w-BeO structure. Subsequently, the z-BeO phase transforms to the r-BeO phase at 120 GPa. The calculated transition pressures from w-BeO to z-BeO and from z-BeO to r-BeO are respectively higher and lower than those reported by Park *et al* [19]. The latter calculations predict the first transformation at 91 GPa and the second at 147 GPa.

3.2. Phonons in the w-BeO phase

The primitive cell of the w-BeO structure contains four atoms (2 f.u.) which give rise to 12 phonon branches. The phonon dispersion curves along high-symmetry points calculated at zero pressure are shown in figure 1. They are compared to the experimental data measured at room temperature by inelastic x-ray scattering [33]. The calculated acoustic branches remain very close to the experimental data. Discrepancies between experimental and theoretical phonons are observed mostly for high-frequency optic modes in the Γ-X and Γ-A directions.

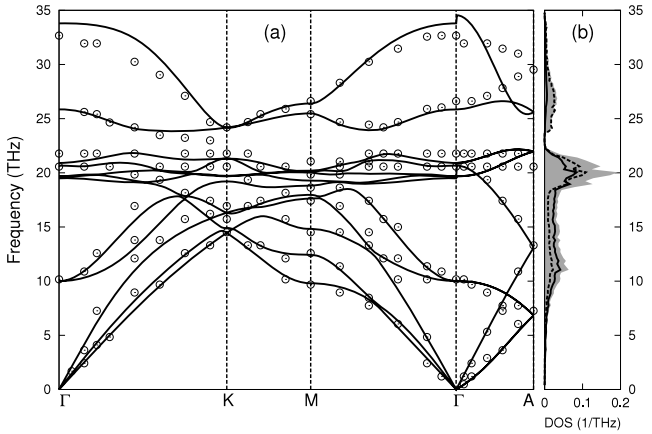

Figure 1. (a) Calculated phonon dispersion relations of the w-BeO phase. Experimental data from inelastic x-ray scattering [33] measured at room temperature are shown as open symbols. (b) Total and partial phonon densities of states (DOS). Contributions to total DOS (shaded area) from Be and O atoms are denoted by solid and dotted lines, respectively.

Figure 1(b) shows the total and partial phonon densities of states (DOS). The partial DOS describes the contribution to the density of states for the selected atom. The high-frequency optical phonons are dominated by the dynamics of light Be atoms and this part of the vibration is separated from the lower lying mixed Be and O vibrations by a small gap. Such a gap, which for the w-BeO crystal amounts to about 1 THz, is typical for crystals having the wurtzite-type structure, e.g. AlN [26].

At the Γ-point of the Brillouin zone the phonon modes in the w-BeO structure decompose according to the irreducible representations characteristic for the C_{6v}^4 space group:

$$\Gamma_{opt} = A_1 + 2B_1 + E_1 + 2E_2 \qquad \text{and} \qquad \Gamma_{ac} = A_1 + E_1$$

for the optical and acoustic modes, respectively. The

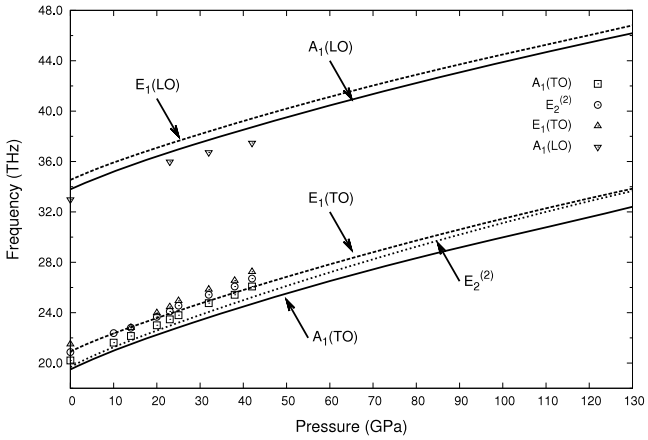

Figure 2. Pressure dependence of the Γ-point optical frequencies in w-BeO crystal. Solid, dashed and dotted curves represent A_1, E_1 and $E_2^{(2)}$ modes, respectively. Experimental data [6] are denoted by open symbols. Squares, down-triangles, up-triangles and circles are assigned to A_1 (TO), A_1 (LO), E_1 (TO) and $E_2^{(2)}$ modes, respectively.

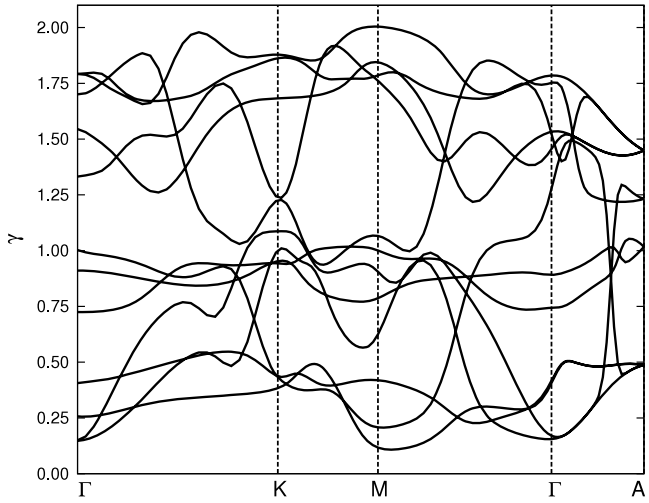

Figure 3. Mode Grüneisen parameters of w-BeO structure calculated according to equation (1).

Table 2. Comparison of the optical modes frequencies (in THz) at the Brillouin zone center of w-BeO crystal.

Mode	This work	Exp. [4]	Exp. [27]	Exp. [6]	Exp. [33]
$E_2^{(1)}$	10.01	10.20	10.14	10.14	10.12
A_1 (TO)	19.50	20.52	20.34	20.46	20.34
$E_2^{(2)}$	19.68	20.52	20.52	20.46	20.49
E_1 (TO)	20.91	21.75	21.66	21.69	21.68
A_1 (LO)	33.79	32.55	32.43	32.85	32.42
E_1 (LO)	34.55	32.85	32.91	—	32.87

Table 3. Calculated and experimental mode Grüneisen parameters for the Γ-point optical modes in the w-BeO phase.

Mode	This work	Exp. [6]
$E_2^{(1)}$	0.15	0.04
A_1 (TO)	1.70	1.69
$E_2^{(2)}$	1.79	1.63
E_1 (TO)	1.54	1.88
A_1 (LO)	0.91	0.98
E_1 (LO)	0.90	—

optical phonons A_1 and E_1 are Raman- and infrared-active, while the E_2 mode is only Raman-active. Modes B_1 are silent. Since BeO has a mixed ionic–covalent bonding, the macroscopic electric field splits the infrared-active modes A_1 and E_1 to transverse A_1 (TO), E_1 (TO) and longitudinal A_1 (LO), E_1 (LO) components. The E_1 mode is due to an opposite motion of cationic and anionic sublattices, with vibrations perpendicular to the c axis. The A_1 mode involves correlated movement of BeO bonds along the c axis, with atoms in a given sublattice vibrating opposite to each other. The calculated frequencies of the above modes at zero pressure are listed in table 2 and compared with experiments. Theoretical TO frequencies are close to those measured by Raman spectroscopy [4, 6, 27, 29, 30] and inelastic x-ray scattering [33] and only a small underestimation of about 0.8–1 THz can be observed. Frequencies of LO modes are higher than the respective experimental values by about 0.9–1.7 THz. This overestimation is mainly due to the approximated value of ϵ_∞ and the values of the effective charges which have been applied to produce the LO modes.

The influence of external pressure on the optical frequencies in the w-BeO crystal is shown in figure 2. A comparison with the experimental data measured by Raman spectroscopy [6] is made. These experiments were performed up to 41.5–55 GPa. The pressure dependence of the $E_2^{(1)}$ mode is not shown as the frequency of this mode (10.01 THz) remains constant upon compression. Such behavior of the $E_2^{(1)}$ mode frequency versus pressure was observed experimentally as well. The remaining mode frequencies increase gradually with compression. When the pressure is increased up to 40 GPa, the experimental LO–TO splitting of the A_1 mode decreases by about 1.4 THz, while the calculated decrease in the splitting is nearly three times smaller. The calculated splitting of the E_1 mode shows similar behavior upon pressure. Present calculations are expected to produce a weak or practically constant dependence of the mode splitting versus pressure due to the approximations applied. Therefore, the calculated LO–TO splitting is governed mainly by changes of the crystal volume with compression which affect predominantly the TO modes.

The volume dependence of the phonon frequencies, described by the mode Grüneisen parameter, exhibits a quite complex nature which is shown in figure 3. Theoretical $\gamma(\mathbf{k}, j)$ of the optical modes at the Brillouin zone center are compared with the available experimental data [6] in table 3. The calculated values agree well with those measured by high-pressure Raman spectroscopy, except the $E_2^{(1)}$ mode for which a significantly higher value is predicted by theory. Parameters $\gamma(\mathbf{k}, j)$ are positive for all phonon branches, indicating that the wurtzite structure of BeO should exhibit a *normal* thermal expansion. A Brillouin zone integration of the mode Grüneisen parameters yields an average value of $\gamma = 1.04$.

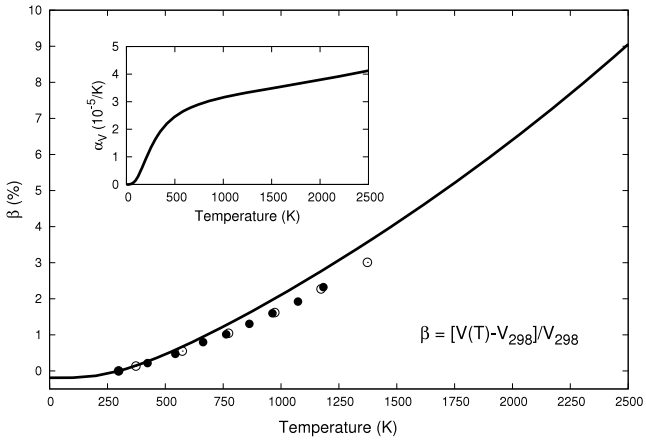

Figure 4. Volume thermal expansion of w-BeO crystal. Solid and open symbols indicate experimental data taken from [3] and [5], respectively. The inset shows the calculated volume thermal expansion coefficient using equation (9).

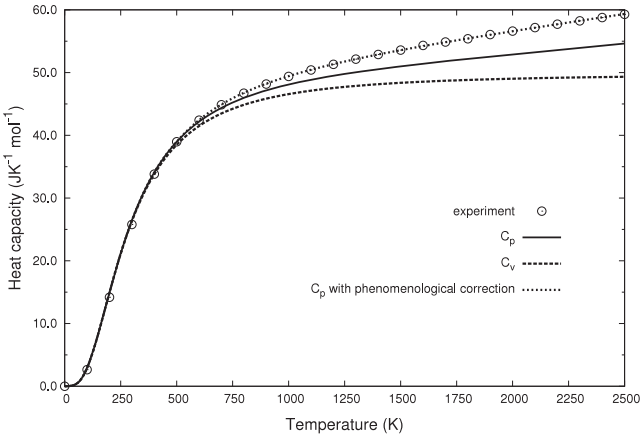

Figure 5. Theoretical and experimental heat capacities of BeO. Experimental data (open symbols) are taken from [7] and [8]. Dashed curve represents calculated C_V according to the harmonic approximation. Solid and dotted curves denote C_p obtained within and beyond the quasiharmonic approximation, respectively.

3.3. Thermal properties of the w-BeO phase

The thermal expansion of the w-BeO crystal can be directly determined from the free energy given by equation (5). The minimum of the $F(V, T)$ curve corresponding to equilibrium volume at a given T shifts to larger values with increasing temperature. The volume thermal expansion expressed in the following form:

$$\beta = \frac{\Delta V}{V_{298}} = \frac{V(T) - V_{298}}{V_{298}} \tag{11}$$

is plotted in figure 4. The symbol V_{298} denotes the crystal volume at 298 K. Good agreement between theoretical expansion and that obtained in experiments [3, 5] is achieved at temperatures not exceeding 700 K. At higher temperatures, the difference between theoretical and experimental β reaches 0.6%. The inset in figure 4 shows the temperature dependence of the volume thermal expansion coefficient calculated according to the Grüneisen relationship (9). One has to note that the expansivity exhibits the same temperature behavior as the heat capacity C_V. Between room temperature and 1200 K, the average value of α_V equals 2.78×10^{-5} K^{-1} as compared to 2.66×10^{-5} K^{-1} and 2.77×10^{-5} K^{-1} given by experiment [3] and other theoretical calculations [23], respectively. It should be noted that, for crystals with a noncubic symmetry, one can expect anisotropic thermal expansion. Measurements performed by Iwanaga *et al* [5] indicate rather small anisotropy in the thermal expansivity of the w-BeO structure ($\alpha_\perp/\alpha_\parallel = 1.11$) as compared to other wurtzite-type crystals (CdSe, CdS, ZnO).

The thermal expansivity results in the difference between C_V and C_p, the latter usually measured in experiments. The term $\alpha_V^2 BVT$ accounts for the lattice anharmonicity. It is relevant at higher temperatures where the difference between C_V and C_p can be significant. In many materials the standard Grüneisen formalism, in which phonon frequencies depend explicitly only on volume and not on temperature, may be insufficient to explain the behavior of C_p at very high temperatures. It occurs that for the BeO crystal one has to go beyond the Grüneisen approximation to fit the experimental C_p [7, 8] at elevated temperatures. This indicates that the BeO lattice anharmonicity can also be due to temperature dependence of the phonon frequencies. This effect cannot be treated theoretically within the present approach and therefore one has to include phenomenological corrections. The difference between measured and theoretical heat capacities at constant pressure (ΔC_p) could be reasonably approximated for temperatures $T \geqslant T_0$ by the following function:

$$\Delta C_p = A_0 + A_1(T - T_0) + A_2(T - T_0)^2, \tag{12}$$

with $A_0 = -0.016$ J (mol K)$^{-1}$, $A_1 = 2.81 \times 10^{-3}$ J (mol K^2)$^{-1}$, $A_2 = -2.23 \times 10^{-7}$ J (mol K^3)$^{-1}$ and $T_0 = 500$ K. These corrections are insignificant below T_0 and the experimental data are also well reproduced by C_V, which can be seen in figure 5. The applied correction becomes meaningful above 1000 K, when substantial difference between experiment and quasiharmonic theory is found.

Figure 6(a) shows the mean-squared amplitude of atomic vibrations calculated versus temperature and at ambient pressure for Be and O atoms. The mean-squared displacements of a given atom constitute a second-rank symmetric tensor and they can be expressed by the diagonal and off-diagonal partial phonon density of states [38]. Due to the hexagonal symmetry of the w-BeO crystal the tensor of thermal motions has two independent components, i.e. $U_{11} = U_{22} = 2U_{21}$ and U_{33}. Experimental U_{ij} from [3] are shown for comparison as well. It is obvious that oxygen atoms exhibit smaller mean-squared displacements than beryllium atoms since the oxygen mass is nearly twice the mass of beryllium. Theoretical U_{11} and U_{33} of both Be and O atoms are underestimated as compared to the respective experimental values. A discrepancy between experiment and theory is larger at room temperature and it becomes smaller at elevated temperatures. Moreover, at higher temperatures the component U_{33}(Be) falls in the range predicted by theory for

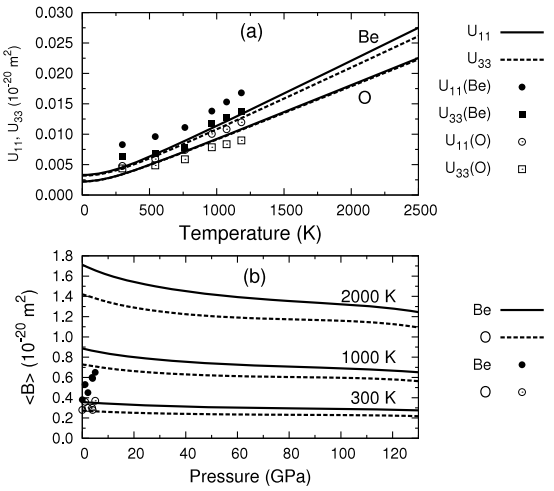

Figure 6. Mean-squared displacements versus temperature for cations and anions in BeO crystal. Calculated U_{11} and U_{33} components are shown as solid and dashed curves, respectively. (b) Isotropic temperature factors for Be (solid curve) and O (dashed curve) versus external pressure. Experimental data for Be (solid symbols) and O (open symbols) are taken from [3].

Table 4. Calculated and experimental [3] anisotropy in thermal motion of BeO atoms. Anisotropy is denoted as $\eta = U_{11}/U_{33}$.

	η (Be)		η (O)	
T (K)	Theory (%)	Exp. (%)	Theory (%)	Exp. (%)
300	5	31	1	9
1183	5	22	1	33

U_{11}(Be). Much smaller deviations between the calculated and measured mean-squared displacements are found for oxygen atoms. The component U_{11} is greater than U_{33}, resulting in the anisotropy of the thermal motion. Although the anisotropy observed in experiment is confirmed by the present calculations, the magnitude of the anisotropy given by theory is significantly smaller than that determined experimentally. The measurements give a pronounced difference between U_{11}(Be) and U_{33}(Be) even at room temperature, while the calculations result in a rather small anisotropy (see table 4 for details). Contrary to experiment, the thermal motion of oxygen atoms is predicted to be practically isotropic. One has to note that the calculated anisotropy of both Be and O atoms is constant versus temperature. This is due to the harmonic approximation which was applied to obtain the mean-squared amplitude of atomic vibrations. From the experimental point of view, the anisotropy of oxygen vibrations increases with increasing temperature, while the thermal motion of Be atoms tends to be more isotropic at high temperatures. The anisotropy in thermal motions can account for the anisotropy of the thermal expansivity and for a decrease of the c/a ratio with increasing temperature, which were observed experimentally in the wurtzite structure of BeO by Iwanaga *et al* [5]. The slope of theoretical mean-squared displacements could be used to estimate the Debye temperature (Θ_D) of the BeO crystal. The calculated Θ_D amounts to 1100 K as compared to 1280 K, the latter reported by Cline *et al* [10].

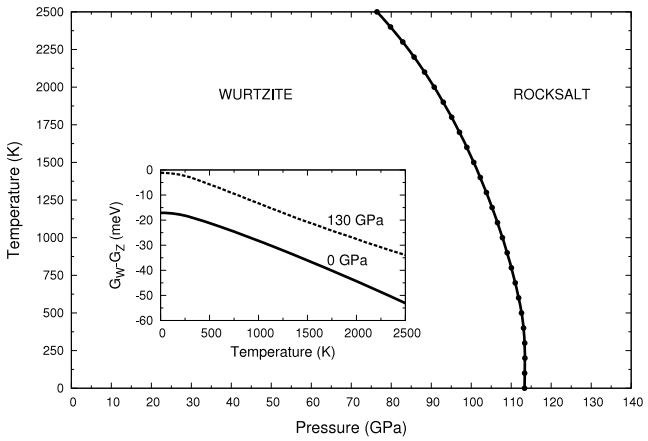

Figure 7. Calculated (p, T) phase diagram of BeO. Inset: difference in the Gibbs free energies between w-BeO and z-BeO phases versus temperature at ambient pressure (solid line) and 130 GPa (dashed line).

Experimental data of Hazen *et al* [3] indicate that the vibrational amplitudes can be pressure-dependent. The measurements were carried out up to 5 GPa at room temperature and the isotropic temperature factors $\langle B \rangle$ of both Be and O atoms have been given. To compare the present calculations with the reported data, the temperature factors were evaluated according to the following relation:

$$\langle B \rangle = 8\pi^2 \langle U \rangle, \tag{13}$$

with $\langle U \rangle$ denoting the trace of the tensor U_{ij}. The pressure dependence of $\langle B \rangle$ is shown in figure 6(b). Again, a discrepancy between theory and experiment is encountered for Be atoms. At room temperature, calculations predict a very small decrease of $\langle B \rangle$(Be) with compression, while the experimental data show the opposite behavior. Calculations meet the experiment only at ambient pressure, where the theoretical temperature factors either for Be or O atoms are similar to those found in experiment. A decrease of $\langle B \rangle$ with increasing pressure is more pronounced at elevated temperatures. On the other hand, the higher the pressure the smaller the change in $\langle B \rangle$ is observed.

4. Phase diagram of BeO

In the framework of the quasiharmonic approximation one is able to construct the complete phase transition diagram from the sets of the Gibbs free energy plots. The phase transition diagram is shown in figure 7. This diagram shows the regions of the most stable structures of the BeO crystal. At low pressures and for temperatures below 2500 K the wurtzite structure of BeO is the most stable one. At higher pressures and temperatures the rocksalt phase of BeO becomes stable. Figure 8 shows the behavior of the Gibbs free energies versus increasing temperature and pressure for wurtzite and rocksalt phases. At the given temperature and pressure, the curve crossing indicates the coexistence of w-BeO and r-BeO phases. For example, at zero temperature the transition pressure equals 113 GPa, while at 2500 K it decreases to 76 GPa. It should be

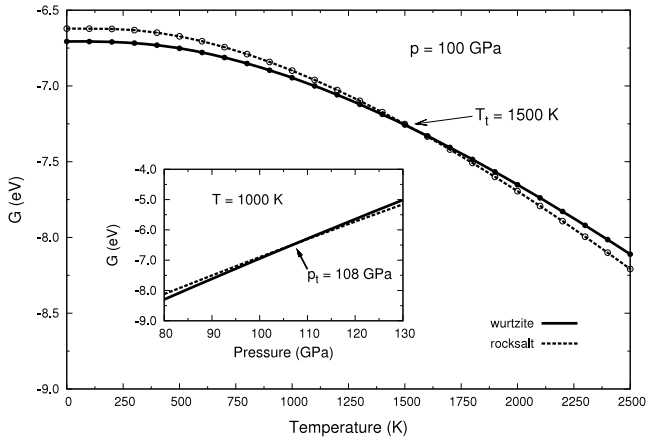

Figure 8. Variation of the Gibbs free energies with temperature at 100 GPa for w-BeO and r-BeO phases. Inset: Gibbs free energies of w-BeO and r-BeO phases versus pressure at 1000 K. Solid and dashed curves are assigned to w-BeO and r-BeO structures, respectively.

noted that no zinc blende structure appears in the calculated (p, T) diagram. Hence, no phase transition either from w-BeO to z-BeO or from z-BeO to r-BeO takes place. The wurtzite phase transforms directly into the rocksalt phase and the higher the temperature the lower the transition pressure. The zinc blende phase of BeO is only slightly higher in energy than the wurtzite phase, as can be seen in the inset of figure 7. The difference between the Gibbs free energies of w-BeO and z-BeO increases with increasing temperature and decreases with increasing pressure, i.e. the temperature stabilizes the wurtzite phase over the zinc blende phase. The role of pressure is opposite, which is also known from many calculations performed with a neglected temperature effect. The quasiharmonic calculations support theoretical predictions of Cai *et al* [21], which also suggest the instability of the z-BeO phase as far as the energetic stability is concerned. Thus, the intermediate phase having the zinc blende structure has to be excluded from the transition sequence proposed previously for the BeO crystal by some first-principles calculations.

5. Summary and conclusions

The structural, vibrational and thermodynamic properties of BeO crystals have been studied by the quasiharmonic approximation with density functional theory. The quantities calculated at the zero-temperature limit remain in the range determined by earlier theoretical studies. Dispersion relations of phonons at ambient pressure show good agreement with recent x-ray scattering experiments. An increase in phonon frequencies with increasing pressure is observed. This effect is mainly due to a decrease of the crystal volume with compression, which involves a diminishing of the interatomic distances and an increase of the force constants. Therefore, the zone-center optical phonon mode frequencies shift upward with increasing pressure, which is also seen experimentally by Raman and infrared spectroscopes.

Most of the calculated thermodynamic properties of the w-BeO structure stay in acceptable agreement with the available experimental data. Despite some inconsistency between theory and experiment which was found for amplitudes of thermal vibrations, the results of present calculations can give some insight into the anisotropy in the thermal expansivity of the w-BeO crystal. This anisotropy is likely to be partly driven by the anisotropy of the thermal motion of atoms.

The phonon frequencies are expected to be not only volume-but also temperature-dependent since the isobaric heat capacity obtained within the quasiharmonic approximation is unable to account for the experimental data at very high temperatures. Hence, the anharmonicity in the lattice vibrations of BeO can be only partly explained within quasiharmonic theory.

The calculated (p, T) diagram predicts the pressure-driven phase transition from wurtzite to rocksalt structure. The increasing temperature lowers the value of the transition pressure. Results given by the quasiharmonic approximation supply previous theoretical studies aimed at structural stability of BeO crystal. However, they exclude the intermediate zinc blende structure from the phase diagram, at least in the theoretically investigated range of temperatures and pressures. It should be mentioned that the wurtzite–zinc blende–rocksalt transition sequence was also not confirmed by the approach of quasiharmonic theory applied for wurtzite-type AlN compound [26].

Acknowledgments

Krzysztof Parlinski is warmly acknowledged for many stimulating discussions. Calculations have been partly performed using the computer facilities of the Interdisciplinary Modeling Center (ICM), Warsaw University, Poland, grant no. G28-12.

References

[1] Slack G A and Austerman S B 1971 *J. Appl. Phys.* **42** 4713
[2] Roessler D M, Walker W C and Loh E 1969 *J. Phys. Chem. Solids* **30** 157
[3] Hazen R M and Finger L W 1986 *J. Appl. Phys.* **59** 3728
[4] Loh E 1968 *Phys. Rev.* **166** 673
[5] Iwanaga H, Kunishige A and Takeuchi S 2000 *J. Mater. Sci.* **35** 2451
[6] Jephcoat A P, Hemley R J, Mao H K, Cohen R E and Mehl M J 1988 *Phys. Rev.* B **37** 4727
[7] Victor A C and Douglas T B 1963 *J. Res. Natl Bur. Stand.* A **67** 325
[8] Conway J B and Hein R A 1964 *Nucleonics* **22** 71
[9] Cline C F and Stephens D R 1965 *J. Appl. Phys.* **36** 2869
[10] Cline C F, Dunegan H L and Henderson G W 1967 *J. Appl. Phys.* **38** 1944
[11] Marsh S P 1973 *High Temp.-High Press.* **5** 503
[12] Mori Y, Ikai T and Takarabe K 2003 *Photon Factory Activity Report* vol 20B p 215
[13] Ma Y, Skytt P, Wassdahl N, Glans P, Guo J and Nordgren J 1993 *Phys. Rev. Lett.* **71** 3725
[14] Harada Y, Tokushima T, Takata Y, Takeuchi T, Kitajima Y, Tanaka S, Kayanuma Y and Shin S 2004 *Phys. Rev. Lett.* **93** 017401
[15] Chang K J, Froyen S and Cohen M L 1983 *J. Phys. C: Solid State Phys.* **16** 3475
[16] Chang K J and Cohen M L 1984 *Solid State Commun.* **50** 487

[17] Van Camp P E and Van Doren V E 1996 *J. Phys.: Condens. Matter* **8** 3385
[18] Boettger J C and Wills J M 1996 *Phys. Rev.* B **54** 8965
[19] Park C J, Lee S G, Ko Y J and Chang K J 1999 *Phys. Rev.* B **59** 13501
[20] Milman V and Warren M C 2001 *J. Phys.: Condens. Matter* **13** 241
[21] Cai Y, Wu S, Xu R and Yu J 2006 *Phys. Rev.* B **73** 184104
[22] Amrani B, Hassan F and Akbarzadeh H 2007 *J. Phys.: Condens. Matter* **19** 436216
[23] Song H-F, Liu H-F and Tian E 2007 *J. Phys.: Condens. Matter* **19** 456209
[24] Kern G, Kresse G and Hafner J 1999 *Phys. Rev.* B **59** 8551
[25] Łażewski J, Jochym P T, Piekarz P and Parlinski K 2004 *Phys. Rev.* B **70** 104109
[26] Siegel A, Parlinski K and Wdowik U D 2006 *Phys. Rev.* B **74** 104116
[27] Arguello C A, Rousseau D L and Porto S P 1969 *Phys. Rev.* **181** 1351
[28] Kourouklis G A, Sood A K, Hochheimer H D and Jayaraman A 1985 *Phys. Rev.* B **31** 8332
[29] Devanarayanan S, Morell G and Katiyar R S 1991 *J. Raman Spectrosc.* **22** 311
[30] Morell G, Pérez W, Ching-Prado E and Katiyar R S 1996 *Phys. Rev.* B **53** 5388
[31] Brugger R M, Song K A and Carpenter J M 1967 *J. Phys. Chem. Solids* **28** 249
[32] Ostheller G L, Schmunk R E, Brugger R M and Kearney R J 1968 *Inelastic Neutron Scattering* (Vienna: IAEA) p 315
[33] Bosak A, Schmalzl K, Krisch M, van Beek W and Kolobanov V 2008 *Phys. Rev.* B **77** 224303
[34] Young j A 1966 *Reactor Physics in the Resonance and Thermal Regions* (Cambridge, MA: MIT)
[35] Sahariah M B and Ghosh S 2008 *J. Phys.: Condens. Matter* **20** 395201
[36] Kresse G and Furthmüller J 1999 *Computer code VASP* Vienna, Austria
[37] Kresse G and Furthmüller J 1996 *Phys. Rev.* B **54** 11169
[38] Parlinski K 2008 *Software PHONON* Cracow, Poland
[39] Parlinski K, Li Z-Q and Kawazoe Y 1997 *Phys. Rev. Lett.* **78** 4063
[40] Pick R M, Cohen M H and Martin R M 1970 *Phys. Rev.* B **1** 910
[41] Dal Corso A, Posternak M, Resta R and Baldereschi A 1994 *Phys. Rev.* B **50** 10715
[42] Bernardini F and Fiorentini V 1998 *Phys. Rev.* B **58** 15292
[43] Noel Y, Llunell M, Orlando R, D'Arco P and Dovesi R 2002 *Phys. Rev.* B **66** 214107
[44] Wagner J M and Brechstedt F 2000 *Phys. Rev.* B **62** 4526
[45] Goñi A R, Siegle H, Syassen K, Thomsen C and Wagner J M 2001 *Phys. Rev.* B **64** 035205
[46] Manjón F J, Syassen K and Lauck R 2002 *J. High Press. Res.* **22** 299
[47] Piekarz P, Jochym P T, Parlinski K and Łażewski J 2002 *J. Chem. Phys.* **117** 3340